

# Monte Carlo study of the classical antiferromagnetic $J_1$ - $J_2$ - $J_3$ Heisenberg model on a simple cubic lattice

A.N. Ignatenko,<sup>\*</sup> S.V. Streltsov,<sup>†</sup> and V.Yu. Irkhin<sup>‡</sup>

*M.N. Mikheev Institute of Metal Physics of Ural Branch of Russian Academy of Sciences*

An extensive Monte Carlo study of the classical Heisenberg model on a simple cubic lattice with antiferromagnetic exchange interactions  $J_n$  between the first, second, and third neighbors is performed in a broad region of  $J_2/J_1$ ,  $J_3/J_1$  ratios, and temperature. The character of the phase transitions is analyzed via the Binder cumulant method. The Neel temperature  $T_N$  and the frustration parameter (the ratio  $f = |\theta|/T_N$ ,  $\theta$  being the Curie-Weiss temperature) are calculated. A comparison with the Tyablikov approximation is carried out. The strength of the frustration effects is explored. Possible applications to antiferromagnetic perovskites, such as  $\text{CaMnO}_3$  and  $\text{HgMnO}_3$ , are discussed.

Keywords: J1-J2-J3 Heisenberg model; simple cubic lattice; frustration; Monte Carlo simulation; Tyablikov approximation

## I. INTRODUCTION

The thermodynamic behavior of frustrated spin systems is the classical field of contemporary condensed matter physics [1, 2]. Generally speaking, the quantum antiferromagnetic Heisenberg model has a complicated phase diagram including magnetically ordered and spin-liquid states, the latter being extensively investigated in the two-dimensional case [3, 4]. The situation for the simple cubic lattice with frustrated exchange interactions is also interesting and complicated. In particular, the results on the formation of spin-liquid phase are somewhat controversial [5, 6].

There are a number of experimental examples of related real materials such as perovskites, in particular antiferromagnetic perovskites  $\text{AMnO}_3$ , where Mn ions form a simple cubic lattice,  $A$  is a simple metal, e.g., Ca or Hg. In  $\text{CaMnO}_3$ , the Neel temperature  $T_N$  is only 125 K, while absolute value of the Curie-Weiss temperature is much higher,  $\theta \simeq -500$  K [7]. In the recently synthesized phase of  $\text{HgMnO}_3$ , a low  $T_N = 60$  K was experimentally obtained, and the paramagnetic Curie temperature is  $-153$  K [8]. The exchange parameters calculated in Ref. 9 at Hubbard's  $U = 3$  eV are  $J_1 = 28.55$  K,  $J_2 = 3.95$  K,  $J_3 = -0.23$  K for  $\text{CaMnO}_3$  and  $J_1 = 13.93$  K,  $J_2 = 4.18$  K,  $J_3 = 0.70$  K for  $\text{HgMnO}_3$ . The decrease in  $T_N$  seems to be caused by a moderate frustration of exchange interactions between the nearest and next-nearest neighbors — competition of magnetic orders with wave vectors  $(\pi, \pi, \pi)$  and  $(0, \pi, \pi)$ .

From the pure theoretical point of view, the Heisenberg model with frustrated exchange interactions provides a unique example of the spin model where collinear configurations dominate quasi-classically for arbitrary ratios of the antiferromagnetic exchange parameters. This makes it an excellent playground for testing various theoretical

and numerical approaches such as functional renormalization group in spin [10] and pseudofermion [5] versions, nonlinear spin wave theory [11–13], series expansion [6], quantum [5, 14] and classical [15, 16] Monte Carlo simulations. In spite of this, no extensive Monte Carlo simulation for general ratios of exchange parameters was performed to the best of our knowledge. Here we perform such calculations taking into account exchange interactions up to the third neighbors in the classical model, which does not suffer from the sign problem for  $J_2 \neq 0$  as the quantum model does [5]. Besides that, it provides more clear and simple picture due to absence of the spin-liquid phase.

## II. MODEL AND CALCULATION METHODS

The Monte-Carlo method is widely used to treat magnetic systems with localized spins (see, e.g., recent works [17–20]). Here we apply this method to the classical Heisenberg Hamiltonian on a simple cubic lattice

$$H = \frac{1}{2} \sum_{ij} J_{ij} \mathbf{S}_i \cdot \mathbf{S}_j,$$

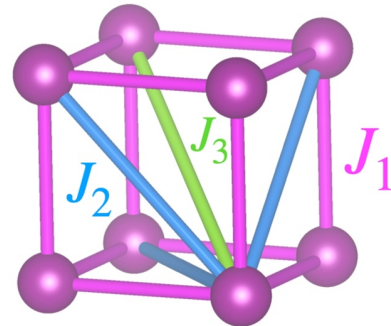


Figure 1: Illustration of the exchange interaction parameters ( $J_1, J_2, J_3$ ) used in the model calculations.

<sup>\*</sup> Email: andrey-n-ignatenko@mail.ru

<sup>†</sup> Email: streltsov@imp.uran.ru

<sup>‡</sup> Email: valentin.irkhin@imp.uran.ru

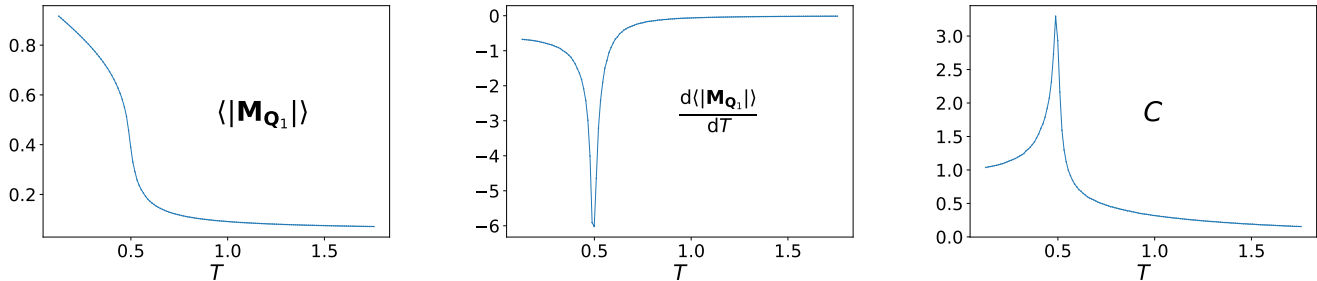


Figure 2: Average absolute value of the total  $\mathbf{Q}_1$ -vector magnetic moment  $|\mathbf{M}_{\mathbf{Q}_1}|$  as a function of temperature for  $J_2 = 0.391$ ,  $J_3 = 0.05$  and  $L = 10$  (left panel); its derivative on temperature (middle panel). Temperature dependence of the specific heat for the same parameters (right panel).

where each bond is counted twice in the summation, spins  $\mathbf{S}_i$  are unit vectors,  $\mathbf{S}_i^2 = 1$  and there is exchange interaction between the first ( $J_1 > 0$ ), the second ( $J_2 \geq 0$ ), and the third ( $J_3 \geq 0$ ) neighbors, see Fig. 1. Below we suppose that the exchange parameters and temperature are all measured in units of  $J_1$ , so that  $J_1 = 1$ . All the possible elementary classical ground states are collinear states described by some magnetic wave vector  $\mathbf{q}$ . The state with staggered order has  $\mathbf{q} = \mathbf{Q}_0 = (\pi, \pi, \pi)$ . For the stripe order state,  $\mathbf{q}$  equals to one of the vectors

$$\mathbf{Q}_1^{(1)} = (0, \pi, \pi), \quad \mathbf{Q}_1^{(2)} = (\pi, 0, \pi), \quad \mathbf{Q}_1^{(3)} = (\pi, \pi, 0).$$

For the order with alternating ferromagnetic planes  $\mathbf{q}$  equals to one of the vectors

$$\mathbf{Q}_2^{(1)} = (\pi, 0, 0), \quad \mathbf{Q}_2^{(2)} = (0, \pi, 0), \quad \mathbf{Q}_2^{(3)} = (0, 0, \pi).$$

Note that there are also more complex non-collinear ground states that comprise of a mixture of those elementary ground states that are degenerate in energy (see, e.g., Ref. [21]). For  $J_3 < 1/4$  the  $\mathbf{Q}_0$ -state is stable for  $J_2 < J_3 + 1/4$ , while for higher  $J_2$  the  $\mathbf{Q}_1$ -state becomes stable. For  $J_3 > 1/4$  the  $\mathbf{Q}_0$ -state is stable for  $J_2 < 1/2$ , and the  $\mathbf{Q}_2$ -state is stable for higher  $J_2$ . In this paper we restrict ourselves to the case  $J_3 < 1/4$ .

Our study of the  $J_1$ - $J_2$ - $J_3$  cubic lattice Heisenberg model is based on the classical Monte-Carlo simulation. The standard Metropolis Monte Carlo algorithm applied to the Heisenberg model includes the following steps:

1. Generate a random lattice site.
2. For this lattice site generate a new spin direction with uniform probability distribution.
3. Accept the new state with the probability  $\exp(-\beta\Delta E)$ , where  $\Delta E$  is the change of the energy between new and old state and  $\beta$  is the inverse temperature.

However, because of multiple cavities in the energy landscape of the frustrated systems, the Metropolis algorithm

works poorly. The performance is especially bad at low temperatures where the algorithm takes exponentially large number of steps in order to escape from a local minimum of the energy.

Because of this drawback of the Metropolis algorithm we use in the calculations the so called “heat bath” algorithm defined by the following steps

1. Generate a random lattice site  $i$ .
2. Calculate the field  $\mathbf{h}_i = -\sum_j J_{ij}\mathbf{S}_j$  produced by all other spins at the lattice site  $i$ .
3. For this lattice site generate a new spin direction with the probability distribution  $\rho(\mathbf{S}_i) \propto \exp(\beta\mathbf{h}_i \cdot \mathbf{S}_i)$  and accept it.

Our implementation of the “heat bath” Monte Carlo algorithm uses C++ libraries ALPSCORE (<https://alpscore.org/>, see also Ref. 22) and Boost (<https://www.boost.org/>), the later being basically exploited for the Mersenne Twister pseudorandom number generator. The simulations are performed for finite cubic supercells containing  $L = 10, 20, 30, 40$  number of lattice periods and  $N = L^3$  number of atoms. The periodic boundary conditions are used. To reach the statistical convergence for fluctuating observables, such as total energy and sublattice magnetizations, the algorithm performs  $(2 - 3) \times 10^5$  complete sweeps of the lattice, where, by definition, one lattice sweep takes  $L^3$  elementary Monte Carlo steps, so that on average each lattice site is touched once. The calculation of Binder cumulants (see below) requires much larger number of sweeps  $(3 - 4) \times 10^6$ .

### III. RESULTS AND DISCUSSION

As the Monte Carlo algorithm operates, a set of observables is calculated and their averages are accumulated.

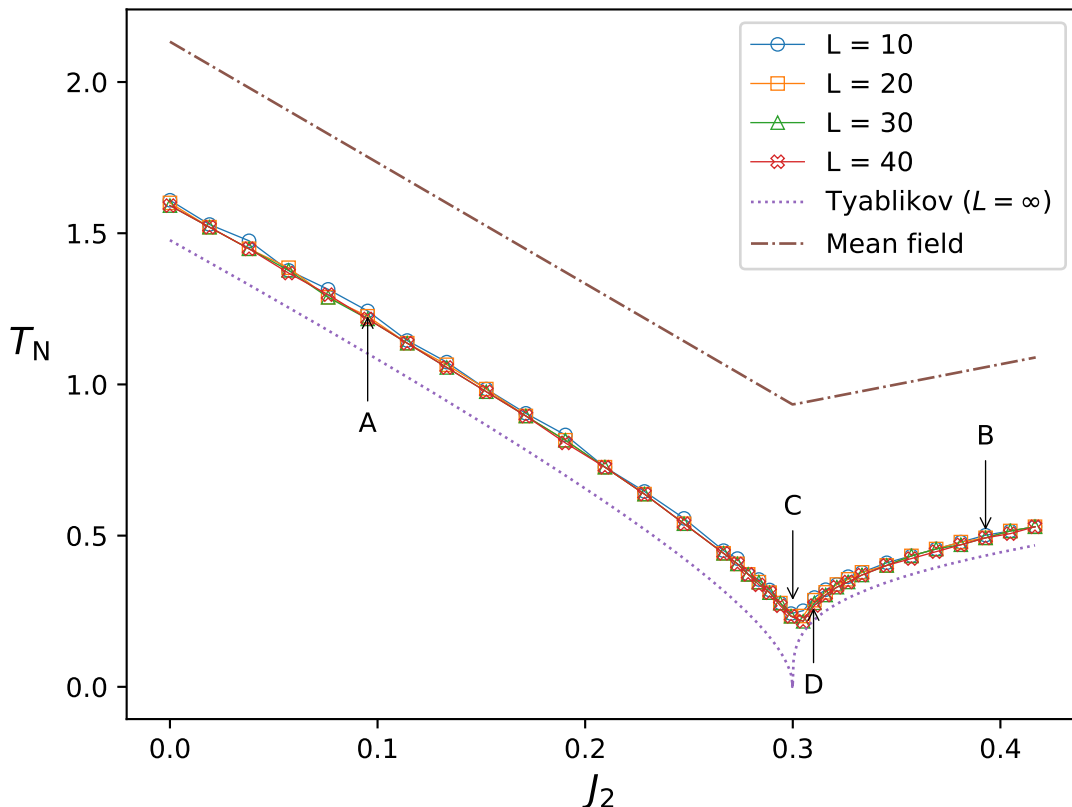


Figure 3: The Neel temperature as a function of  $J_2$  calculated in the Monte Carlo simulation for  $J_3 = 0.05$  and lattice sizes  $L = 10, 20, 30, 40$  (empty markers connected with solid lines) and compared with the Tyablikov approximation,  $L = \infty$  (bottom dotted line) and the mean field theory (upper dash-dotted line). Arrows point to Neel temperatures for  $J_2 = 0.95$  (point A),  $0.393$  (point B),  $0.3 = J_2^{(c)}$  (point C), and  $0.31$  (point D).

Our set of observables is

$$E, E^2, \mathbf{M}_{\mathbf{Q}_0}, M_{\mathbf{Q}_0}^2, |\mathbf{M}_{\mathbf{Q}_0}|, M_{\mathbf{Q}_0}^4, EM_{\mathbf{Q}_0}^2,$$

$$\mathbf{M}_{\mathbf{Q}_1^{(a)}}, a = 1 \dots 3, \quad M_{\mathbf{Q}_1}^2 = \sum_{a=1}^3 \mathbf{M}_{\mathbf{Q}_1^{(a)}} \cdot \mathbf{M}_{\mathbf{Q}_1^{(a)}},$$

$$|\mathbf{M}_{\mathbf{Q}_1}| = \sqrt{M_{\mathbf{Q}_1}^2}, M_{\mathbf{Q}_1}^4, EM_{\mathbf{Q}_1}^2,$$

where  $E = H/N$  is the energy per site and  $\mathbf{M}_{\mathbf{q}} = N^{-1} \sum_i \mathbf{S}_i e^{i\mathbf{q} \cdot \mathbf{r}_i}$  is the total  $\mathbf{q}$ -vector magnetic moment per site. Some useful physical quantities can be expressed in terms of averages of these observables. For example,

$$C = N\beta^2 (\langle E^2 \rangle - \langle E \rangle^2)$$

is the specific heat and

$$\frac{d\langle |\mathbf{M}_{\mathbf{q}}| \rangle}{dT} = \beta^2 \frac{\langle M_{\mathbf{q}}^2 E \rangle - \langle M_{\mathbf{q}}^2 \rangle \langle E \rangle}{2\langle |\mathbf{M}_{\mathbf{q}}| \rangle}$$

is the temperature derivative of the average absolute value of the total non-uniform magnetization for a given

$\mathbf{q}$ -vector. This parameter turns out to be useful in distinguishing magnetically ordered phases from the paramagnetic one. Indeed, simple averages  $\langle \mathbf{M}_{\mathbf{q}} \rangle$  or  $\langle |\mathbf{M}_{\mathbf{q}}| \rangle$  cannot be used for this purpose since the first one is always zero (there is no spontaneous symmetry breaking for finite systems) and the second one is never zero. However, the temperature dependence of  $\langle |\mathbf{M}_{\mathbf{q}}| \rangle$  has an inflection point (see Fig. 2, left panel), corresponding to the minimum of its first derivative (see Fig. 2, middle panel). The sharpness of the minimum increases with increasing system size, and the position of the minimum can be taken as an estimate for the critical temperature of the phase transition between states with  $\mathbf{q}$ -vector magnetic order and without such an order.

Another option is to take the position of the specific-heat maximum (see Fig. 2, right panel) as a transition temperature estimate. An obvious disadvantage of this method is the inability to determine  $\mathbf{q}$ -vector characterizing the magnetic order. Moreover, the maximum does not necessarily correspond to a phase transition, for example, in two-dimensional and layered systems the spe-

cific heat has a broad maximum at a temperature proportional to in-layer exchange parameter [23]. Therefore we prefer to determine the transition temperature from the  $\langle |\mathbf{M}_{\mathbf{q}}| \rangle$  inflection point. Nevertheless, for the present system both the methods give almost identical critical-temperature estimates.

We compare the critical temperature determined from our Monte Carlo simulation with the result of the mean-field approach

$$T_N^{(\text{Mean field})} = \frac{|J(\mathbf{q})|}{3},$$

and also with the result of the Tyablikov approximation

$$T_N^{(\text{Tyablikov})} = \frac{1}{3} \left( \int \frac{d^3\mathbf{k}}{(2\pi)^3} \frac{1}{J(\mathbf{k}) - J(\mathbf{q})} \right)^{-1}. \quad (1)$$

In the above equations

$$\begin{aligned} J(\mathbf{k}) &= 2(\cos k_x + \cos k_y + \cos k_z) \\ &+ 4J_2(\cos k_x \cos k_y + \cos k_y \cos k_z + \cos k_z \cos k_x) \\ &+ 8J_3 \cos k_x \cos k_y \cos k_z \end{aligned}$$

(recall that  $J_1 = 1$ ) is the Fourier transform of the exchange parameters.

Fig. 3 shows the dependence of the Neel temperature on  $J_2$  for  $J_3 = 0.05$  and  $L = 10, 20, 30$ , and  $40$ . Importantly, the results for different values of lattice sizes  $L$  are almost the same, so it is likely that they do not change considerably in the limit  $L \rightarrow \infty$ . The Neel temperature has a minimum at the point  $J_2^{(c)} = J_3 + 1/4 = 0.3$  lying at the boundary between  $\mathbf{Q}_0$  (lower  $J_2$ ) and  $\mathbf{Q}_1$  (higher  $J_2$ ) ground states. Everywhere, except for the  $J_2^{(c)}$  neighborhood, the dependence is almost linear and has the same slope as in the mean-field theory. As expected, the latter strongly overestimates the Neel temperature. The deviation from the linear dependence, being more pronounced in the  $\mathbf{Q}_1$ -phase, shows the signs of the frustration, manifested in the enhanced role of fluctuations not accounted in the mean-field theory.

The Tyablikov approximation gives much better results and, except for the  $J_2^{(c)}$  neighborhood, slightly underestimates the Neel temperature. When  $J_2 \rightarrow J_2^{(c)}$  the integral in the Eq. (1) diverges and the Neel temperature vanishes, which is not observed in the Monte Carlo simulation. This discrepancy is explained in non-linear spin-wave theories [24, 25] (in particular, in the self-consistent spin wave theory [26, 27]). The Tyablikov approximation, being an *ad hoc* version of the non-linear spin-wave theory, does not properly account for the self-energy corrections to the magnon spectrum near its hot points. Note that apparent decrease of the Neel temperature in the Monte Carlo simulation near  $J_2^{(c)}$  with increasing  $L$  probably is an artifact of our estimation method owing to its insufficient precision.

To obtain a more precise estimate of the critical temperature and, more importantly, to determine the char-

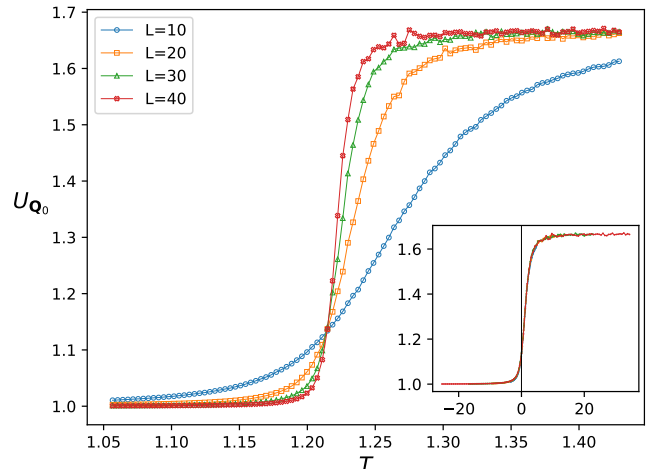


Figure 4: Temperature dependence of the Binder cumulant  $U_{\mathbf{Q}_0}$  in the vicinity of the point A ( $J_2 = 0.095$ ,  $J_3 = 0.05$ ) on Fig. 3 for different lattice sizes  $L$ .  $T_{\text{cross}} = 1.2146$ . The inset shows  $U_{\mathbf{Q}_0}$  as a function of  $x = (T/T_{\text{cross}} - 1)L^{1/\nu}$  with  $\nu = 0.7$ .

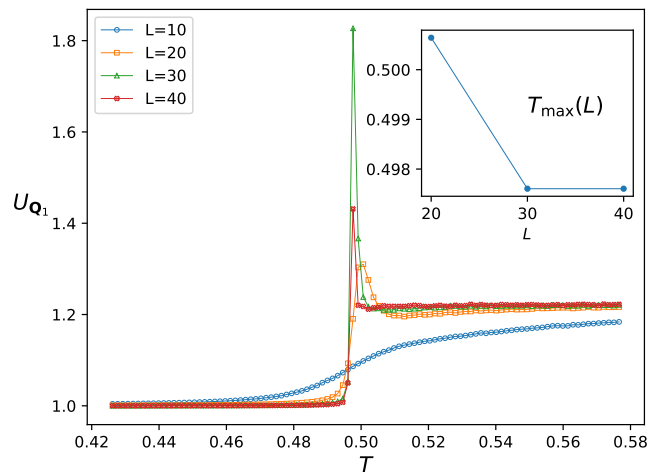


Figure 5: Temperature dependence of the Binder cumulant  $U_{\mathbf{Q}_1}$  in the vicinity of the point B ( $J_2 = 0.393$ ,  $J_3 = 0.05$ ) on Fig. 3 for different lattice sizes  $L$ . The inset shows the positions of the maximums of  $U_{\mathbf{Q}_1}$  as a function of  $L$ .

acter of the phase transition, the Binder cumulant

$$U_{\mathbf{q}} = \frac{\langle \mathbf{M}_{\mathbf{q}}^4 \rangle}{\langle \mathbf{M}_{\mathbf{q}}^2 \rangle^2}$$

can be useful [28]. At low temperatures,  $U_{\mathbf{q}}$  is close to unity in the phase with  $\mathbf{q}$ -vector magnetic order. At high temperatures, when the correlation length  $\xi \ll L$  and

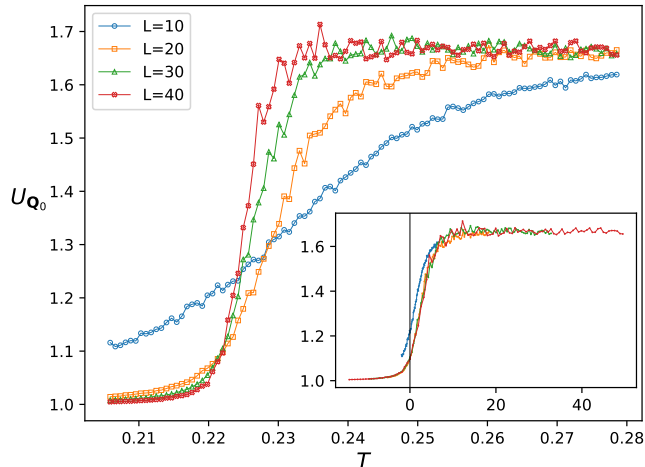


Figure 6: Temperature dependence of the Binder cumulant  $U_{\mathbf{Q}_0}$  in the vicinity of the point C ( $J_2 = J_2^{(c)} = 0.30$ ,  $J_3 = 0.05$ ) on Fig. 3 for different lattice sizes  $L$ ,  $T_{\text{cross}} = 0.222$ . The inset shows  $U_{\mathbf{Q}_0}$  as a function of  $x = (T/T_{\text{cross}} - 1)L^{1/\nu}$  with  $\nu = 0.7$ .

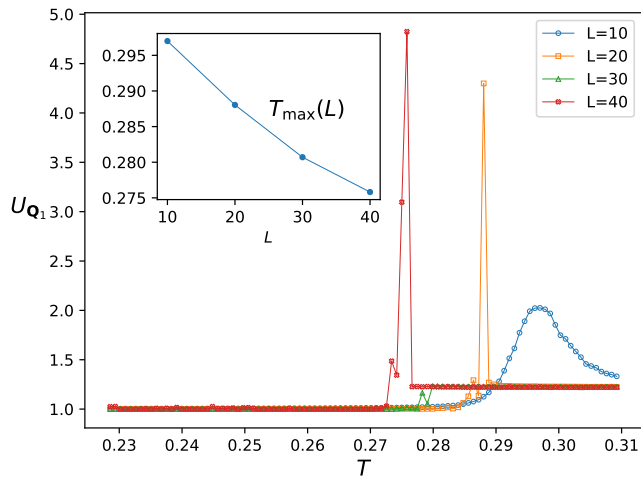


Figure 7: Temperature dependence of the Binder cumulant  $U_{\mathbf{Q}_1}$  in the vicinity of the point D ( $J_2 = 0.31$ ,  $J_3 = 0.05$ ) on Fig. 3 for different lattice sizes  $L$ . The inset shows the positions of the maximums of  $U_{\mathbf{Q}_1}$  as a function of  $L$ .

the components of the order parameter  $\mathbf{M}_{\mathbf{q}}$  become almost statistically independent and fluctuate with Gaussian distribution, application of the Wick theorem gives  $U_{\mathbf{q}} \approx 1 + 2/n$ , where  $n$  is the number of the order parameter components ( $n = 3$  for  $\mathbf{q} = \mathbf{Q}_0$  and  $n = 9$  for  $\mathbf{q} = \mathbf{Q}_1$ ). At intermediate temperatures  $U_{\mathbf{q}}$  interpolates between these two asymptotic values in a way that depends on the character of the phase transition.

In the case of a second-order phase transition, the Binder cumulant follows the scaling relation [29]

$$U_{\mathbf{q}} = b(x = \tau L^{1/\nu}), \quad \tau = T/T_N^\infty - 1, \quad (2)$$

in the critical region  $|\tau| \ll 1$  and at sufficiently large  $L$ , where  $T_N^\infty$  is the critical temperature of the infinite system,  $\nu$  is the critical exponent of the correlation length, and  $b(x)$  is some function that depends on system size  $L$  and temperature only via its argument  $x$ . In particular, the value of the Binder cumulant at  $T = T_N^\infty$  does not depend on  $L$ . Thus, one can determine  $T_N^\infty$  as a cross point of  $U_{\mathbf{q}}(T)$  curves for two or more values of  $L$ . In the case of a first-order phase transition, the Binder cumulant demonstrates a spike [30] connected with the coexistence of two phases at a transition temperature [31, 32]. The spike exists only when  $L$  exceeds some  $L_{\text{min}}$ . Its sharpness increases with increasing  $L$  and the position drifts towards  $T_N^\infty$  [31].

Figs. 4-5 show the temperature behavior of the Binder cumulants  $U_{\mathbf{q}}$  calculated in the vicinity of the points A, B, C, D marked by arrows in Fig. 3.

For the points A and C, the behavior of the Binder cumulant  $U_{\mathbf{Q}_0}$  corresponds to the picture of the second-order phase transition. Curves for different  $L$  are crossed at a single point  $T_{\text{cross}}$ , giving an estimate of  $T_N^\infty$ . When the curves are replotted against  $x = (T/T_{\text{cross}} - 1)L^{1/\nu}$  with  $\nu = 0.7$ , they collapse in agreement with the scaling Eq. (2). Thus measured correlation-length critical exponent  $\nu$  is close to  $\nu_{O(3)} = 0.7112(5)$  of the three-dimensional Heisenberg universality class [33], as it should be.

For the point C, the above picture is true only for  $L = 20, 30$ , and  $40$ , but not for  $L = 10$  where the scaling seems to be broken. We can hypothesize that this means existence of some additional characteristic length scale in Eq. (2), which becomes comparable with  $L = 10$  at the point C and is negligibly small relative to  $L \geq 20$  (a crossover scenario).

For the points B and D, the behavior of the Binder cumulant  $U_{\mathbf{Q}_1}$  corresponds to the picture of the first-order phase transition. There is no scaling, and for  $L > L_{\text{min}}$  we see the spikes, the sharpness of which increases with increasing  $L$ , and the position of the maximum converges towards some value, providing thereby an estimate of  $T_N^\infty$ . For the point B,  $10 \leq L_{\text{min}} < 20$ , and  $L_{\text{min}} < 10$  for the point D. The conclusion about the first-order character of the phase transition is in agreement with the results of the  $4 - \varepsilon$  renormalization group treatment of a phase transition governed by the nine-dimensional order parameter [34]. A similar first-order phase transition was recently observed in the Monte Carlo simulation of the  $J_1$ - $J_2$  Heisenberg model on the body-centered cubic lattice [17].

Fig. 8 shows the dependence of the Neel temperature on  $J_2$  in a wider interval: for  $L = 10$  and for a number of  $J_3$  values increasing from 0 to  $1/4$ . At this larger  $J_2$  scale the nonlinear character of the dependence for  $J_2 > J_2^{(c)}$  is seen more clearly. The value of the Neel

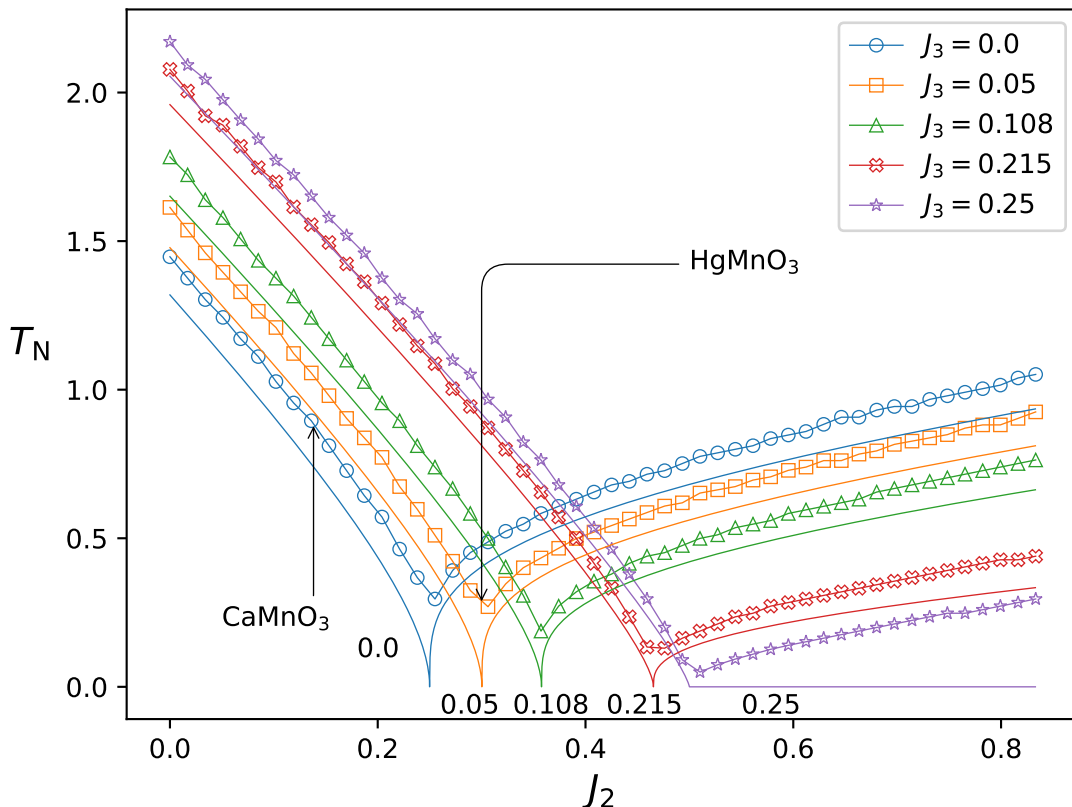


Figure 8: The Neel temperature as a function of  $J_2$  calculated for the number of  $J_3$  values in the Monte Carlo simulation for  $L = 10$  (empty markers connected with solid lines) and compared with the Tyablikov approximation,  $L = \infty$  (solid lines with the same color as the Monte Carlo lines but without markers on them; the corresponding  $J_3$ -values are also indicated by the numbers near the curve's cusps). Arrows indicate Neel temperatures approximately corresponding to ratios  $J_2/J_1$ ,  $J_3/J_1$  for  $\text{CaMnO}_3$  (0.138 and  $-0.008$ ) and  $\text{HgMnO}_3$  (0.3 and 0.05) taken from Ref. 9.

temperature at the minimum decreases with increasing  $J_3$ . At  $J_3 = 1/4$  the Tyablikov approximation exhibits its largest error since the integral in Eq. (1) diverges for all  $J_2 \geq 1/2$ .

To quantify the degree of frustration, Fig. 9 presents for the same parameters as in Fig. 8 the temperature dependence of the frustration ratio

$$f = |\theta|/T_N$$

where  $\theta = -J(\mathbf{q} = 0)/3$  is the Curie-Weiss (paramagnetic Curie) temperature. From this figure it is clear how the effects of the frustration increase with increasing  $J_3$ .

#### IV. CONCLUSIONS

To conclude, the Monte Carlo calculations convincingly demonstrate the importance of fluctuation effects. These effects considerably modify the results obtained

from mean-field theory and the Tyablikov approximation. Therefore, accounting for fluctuations is crucial for the correct interpretation of experimental data on the thermodynamic properties of real antiferromagnetic compounds, particularly frustrated ones. The inclusion of the third-neighbor exchange  $J_3$  into the Hamiltonian increases the maximum of the frustration ratio  $f$  and shifts its position and the position of the Neel temperature's minimum.

The long-range antiferromagnetic exchange interaction with the second and third nearest neighbors becomes especially significant for  $4d$  and  $5d$  transition metal oxides. In these materials, the wave functions of  $d$  electrons are more extended than in the  $3d$  case due to the larger principal quantum number [35].

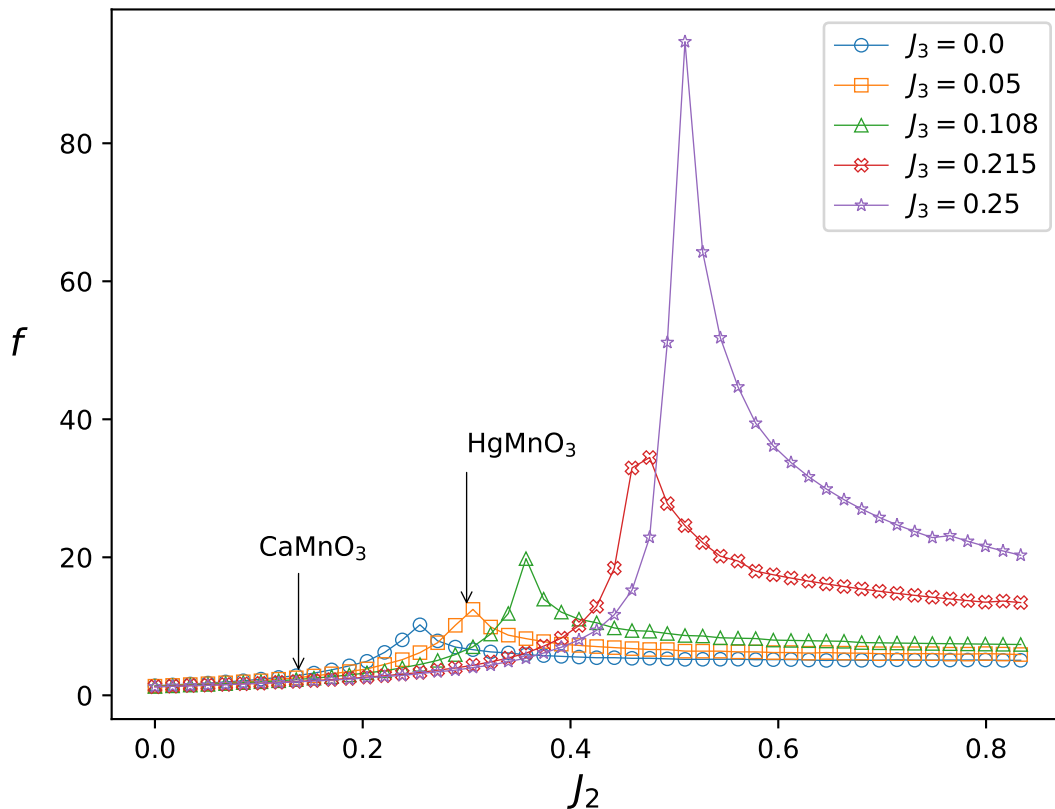


Figure 9: The ratio  $f = |\theta|/T_N$  as a function of  $J_2$  calculated in the Monte Carlo simulation for the same parameters as in Fig. 8

## V. ACKNOWLEDGMENT

We thank E. Komleva for the help with Fig. 1. Computations were performed on the Uran supercomputer at the IMM UB RAS.

## VI. FUNDING

The work was carried out within the framework of the state assignment of the Ministry of Science and Higher

Education of the Russian Federation for the Mikheev Institute of Metal Physics, Ural Branch, Russian Academy of Sciences.

## VII. CONFLICT OF INTERESTS

The authors of this work declare that they have no conflicts of interest.

- 
- [1] H. T. Diep (ed.), *Frustrated Spin Systems* (World Scientific Publishing Co. Pte. Ltd., 2004).  
 [2] D. I. Khomskii and S. V. Streltsov, Magnetic Oxides, in *Encyclopedia of Condensed Matter Physics* (Elsevier, 2024) pp. 98–111.  
 [3] L. Balents, Spin liquids in frustrated magnets, *Nature* **464**, 199 (2010).  
 [4] S.-S. Gong, D. N. Sheng, O. I. Motrunich, and M. P. A. Fisher, Phase diagram of the spin- $\frac{1}{2}$   $J_1$ - $J_2$  Heisenberg

- model on a honeycomb lattice, *Phys. Rev. B* **88**, 165138 (2013).  
 [5] Y. Iqbal, R. Thomale, F. Parisen Toldin, S. Rachel, and J. Reuther, Functional renormalization group for three-dimensional quantum magnetism, *Phys. Rev. B* **94**, 140408 (2016).  
 [6] J. Oitmaa, Frustrated  $J_1 - J_2 - J_3$  Heisenberg antiferromagnet on the simple cubic lattice, *Phys. Rev. B* **95**, 014427 (2017).

- [7] J. Briático, B. Alascio, R. Allub, A. Butera, A. Caneiro, M. T. Causa, and M. Tovar, Double-exchange interaction in electron-doped  $\text{CaMnO}_{3-\delta}$  perovskites, *Phys. Rev. B* **53**, 14020 (1996).
- [8] B. Zhou, S. Qin, T. Ma, X. Ye, J. Guo, X. Yu, H.-J. Lin, C.-T. Chen, Z. Hu, L.-H. Tjeng, G. Zhou, C. Dong, and Y. Long, High-Pressure Synthesis of Two Polymorphic  $\text{HgMnO}_3$  Phases and Distinct Magnetism from 2D to 3D, *Inorganic Chemistry* **59**, 3887 (2020).
- [9] D. A. Myakotnikov, E. V. Komleva, Y. Long, and S. V. Streltsov, Importance of the indirect exchange interaction via  $s$  states in altermagnetic  $\text{HgMnO}_3$ , *Phys. Rev. B* **110**, 134427 (2024).
- [10] D. Tarasevych, A. Rückriegel, S. Keupert, V. Mitsioannou, and P. Kopietz, Spin-functional renormalization group for the  $J_1J_2J_3$  quantum Heisenberg model, *Phys. Rev. B* **106**, 174412 (2022).
- [11] A.-Y. Hu and H.-Y. Wang, Phase transition of the frustrated antiferromagnetic  $J_1$ - $J_2$ - $J_3$  spin-1/2 Heisenberg model on a simple cubic lattice, *Frontiers of Physics* **14**, 13605 (2019).
- [12] V. Y. Irkhin, A. A. Katanin, and M. I. Katsnelson, On the self-consistent spin-wave theory of frustrated Heisenberg antiferromagnets, *Journal of Physics: Condensed Matter* **4**, 5227 (1992).
- [13] K. Majumdar and T. Datta, Zero Temperature Phases of the Frustrated  $J_1$ - $J_2$  Antiferromagnetic Spin-1/2 Heisenberg Model on a Simple Cubic Lattice, *Journal of Statistical Physics*, 714–726 (2010).
- [14] A. W. Sandvik, Critical Temperature and the Transition from Quantum to Classical Order Parameter Fluctuations in the Three-Dimensional Heisenberg Antiferromagnet, *Phys. Rev. Lett.* **80**, 5196 (1998).
- [15] C. Pinettes and H. T. Diep, Phase transition and phase diagram of the  $J_1$ - $J_2$  Heisenberg model on a simple cubic lattice, *Journal of Applied Physics* **83**, 6317 (1998).
- [16] V. T. Ngo, D. T. Hoang, and H. T. Diep, Phase transition in the Heisenberg fully-frustrated simple cubic lattice, *Modern Physics Letters B* **25**, 929 (2011), <https://doi.org/10.1142/S0217984911026632>.
- [17] A. K. Murtazaev, F. A. Kassan-Ogly, M. K. Ramazanov, and K. S. Murtazaev, Study of Phase Transitions in the Antiferromagnetic Heisenberg Model on a Body-Centered Cubic Lattice by Monte Carlo Simulation, *Physics of Metals and Metallography* **121**, 305 (2020).
- [18] I. F. Sharafullin, A. R. Yuldasheva, D. I. Abdrakhmanov, and A. G. Nugumanov, Skyrmion Lattices Phase Driven by Interfacial-Engineered Dzyaloshinskii–Moriya Interaction in Frustrated Antiferromagnetic/Ferroelectric Bilayers, *Physics of Metals and Metallography* **124**, 1697 (2023).
- [19] Z. Zhou, Y. Chen, and W. Li, Onsager Reaction Field Theory for Two-Dimensional Spatially Anisotropic Heisenberg Ferromagnet with the  $x$ -Axis Long-Range Interaction, *Physics of Metals and Metallography* **124**, 1716 (2023).
- [20] S. V. Kolesnikov, E. S. Sapronova, and A. M. Saletsky, Remagnetization of Finite-Length Ferromagnetic Cobalt Atomic Chains, *Physics of Metals and Metallography* **125**, 683 (2024).
- [21] A. N. Ignatenko and V. Y. Irkhin, Frustrated Heisenberg Antiferromagnets on Cubic Lattices: Magnetic Structures, Exchange Gaps, and Non-Conventional Critical Behaviour, *Journal of Siberian Federal University. Mathematics & Physics* **9**, 454 (2016).
- [22] A. Gaenko, A. Antipov, G. Carcassi, T. Chen, X. Chen, Q. Dong, L. Gamper, J. Gukelberger, R. Igarashi, S. Isakov, M. Könz, J. LeBlanc, R. Levy, P. Ma, J. Paki, H. Shinaoka, S. Todo, M. Troyer, and E. Gull, Updated core libraries of the ALPS project, *Computer Physics Communications* **213**, 235 (2017).
- [23] A. N. Vasiliev, O. S. Volkova, E. A. Zvereva, and M. M. Markina, *Low-Dimensional Magnetism* (CRC Press, 2019).
- [24] E. Shender, Antiferromagnetic garnets with fluctuationally interacting sublattices, *JETP* **56**, 178 (1982).
- [25] T. Yildirim, A. B. Harris, and E. F. Shender, Frustration and quantum fluctuations in Heisenberg fcc antiferromagnets, *Phys. Rev. B* **58**, 3144 (1998).
- [26] A. N. Ignatenko and V. Y. Irkhin, The Ising Nematic in the  $J_1$ - $J_2$  Heisenberg Model on a Square Lattice in a Self-Consistent Spin-Wave Theory, *Bulletin of the Russian Academy of Sciences: Physics* **87**, 1601 (2023).
- [27] A. N. Ignatenko, A. A. Katanin, and V. Y. Irkhin, Strong fluctuations near the frustration point in cubic lattice ferromagnets with localized moments, *JETP Letters* **97**, 209 (2013).
- [28] V. Privman (ed.), *Finite Size Scaling and Numerical Simulation of Statistical Systems* (World Scientific, 1990) <https://www.worldscientific.com/doi/pdf/10.1142/1011>.
- [29] K. Binder, Critical Properties from Monte Carlo Coarse Graining and Renormalization, *Phys. Rev. Lett.* **47**, 693 (1981).
- [30] K. Binder and D. P. Landau, Finite-size scaling at first-order phase transitions, *Phys. Rev. B* **30**, 1477 (1984).
- [31] K. Vollmayr, J. D. Reger, M. Scheucher, and K. Binder, Finite size effects at thermally-driven first order phase transitions: A phenomenological theory of the order parameter distribution, *Zeitschrift für Physik B Condensed Matter* **91**, 113 (1993).
- [32] S.-H. Tsai and S. R. Salinas, Fourth-Order Cumulants to Characterize the Phase Transitions of a Spin-1 Ising Model, *Brazilian Journal of Physics* **28**, 58 (1998).
- [33] M. Campostrini, M. Hasenbusch, A. Pelissetto, P. Rossi, and E. Vicari, Critical exponents and equation of state of the three-dimensional Heisenberg universality class, *Phys. Rev. B* **65**, 144520 (2002).
- [34] S. Brazovskii, I. Dzyaloshinskii, and B. Kukharenko, First-order magnetic phase transitions and fluctuations, *Journal of Experimental and Theoretical Physics* **43**, 1178 (1976).
- [35] S. Streltsov and D. Khomskii, Orbital Physics in Transition Metal Compounds: New Trends, *Physics-Uspekhi* **60**, 1121 (2017).